# Beating the wavelength limit: three-dimensional imaging of buried subwavelength fractures in sculpture and construction materials by terahertz time-domain reflection spectroscopy

M. Schwerdtfeger,[1] E. Castro-Camus,[2,*] K. Krügener,[3] W. Viöl,[3] and M. Koch[1]

[1]Philipps-Universität Marburg, Department of Physics, Renthof 5, Marburg 35032, Germany

[2]Centro de Investigaciones en Óptica A.C., Loma del Bosque 115, Lomas del Campestre, León, Guanajuato 37150, Mexico

[3]University of Applied Sciences and Arts, Faculty of Natural Sciences and Technology, Von-Ossietzky-Str. 99, Göttingen 37085, Germany

*Corresponding author: enrique@cio.mx

Received 1 November 2012; revised 5 December 2012; accepted 7 December 2012; posted 10 December 2012 (Doc. ID 179002); published 11 January 2013

We use reflection terahertz spectroscopy to locate and produce three-dimensional images of air gaps between stones that resemble fractures, even of subwavelength thicknesses. This technique is found to be promising tool for sculpture and building damage evaluation as well as structural quality control in other dielectric materials. © 2013 Optical Society of America

*OCIS codes:* 300.6495, 110.6795, 110.3010, 110.6960, 100.6890, 100.6950.

## 1. Introduction

Recently cultural heritage conservation has become a source of challenges to science. Subatomic particle accelerators and various spectroscopy techniques are becoming tools used for dating, authentication, and damage evaluation of various forms of artwork [1,2]. Terahertz time-domain spectroscopy (THz-TDS) [3] is not the exception and has recently been proposed as useful tool in artwork conservation [4,5]. This technique has been used to observe hidden paint layers on canvas [6] and image characters on deteriorated medieval manuscripts [7].

In this article, we present pulsed THz reflection measurements that we use to find buried air gaps of subwavelength thickness within the stone that resemble fractures. Furthermore we describe a method to obtain the thickness of these subwavelength gaps and use it to generate a three-dimensional tomographic reconstruction of their shape. In order to do this, the complex dielectric properties of the stones need to be carefully characterized; therefore, the refractive index and absorption coefficient of a selection of stones that have been used for sculpture as well as for construction of buildings of historical value is also reported.

## 2. Dielectric Properties of Stones

There is a wealth of objects of historical and cultural relevance that are made of stone. From prehistoric tools to sculptures and buildings, stones have been materials that have accompanied mankind through time. Examples of igneous, sedimentary, and metamorphic rocks, shown in Table 1, were selected owing to their use for German art and cultural objects from

1559-128X/13/030375-06$15.00/0

Table 1. Average Refractive Indices of Some Stones

| Short Name | Name | Refractive Index | Validity Range (THz) | Category |
|---|---|---|---|---|
| Marble 1 | Weiße Marianna Marmor | 2.96 | 0.05–1.3 | Metamorphic |
| Marble 2 | Groß Kunzendorfer Marmor | 2.97 | 0.075–1.25 | Metamorphic |
| Sandstone 1 | Baumberger Sandstein | 2.29 | 0.075–0.65 | Sedimentary |
| Sandstone 2 | Roter Wesersandstein | 2.05 | 0.075–0.95 | Sedimentary |
| Sandstone 3 | Obernkirchener Sandstein | 1.95 | 0.075–1.25 | Sedimentary |
| Green Limestone | Anröchter Grünsandstein | 2.51 | 0.05–0.9 | Sedimentary |
| Limestone | Thüster Kalkstein | 2.51 | 0.1–0.4 | Sedimentary |
| Shell Limestone | Kirchheimer Muschelkalk | 2.94 | 0.05–1.2 | Sedimentary |
| Tuff | Weibemer Tuff | 1.78 | 0.05–0.45 | Igneous |

the middle ages up to date. There are a number of well-known buildings of cultural and historical importance, such as the Marmorpalast (The Marble Palace) in Potsdam or the Cathedral of Cologne which are made of such stones. Three samples of each one of these historically relevant stones were obtained from various sources and cut to a thickness of 5 mm. Although some of these rocks share a common generic denomination, such as "marble" or "sandstone," they all present different compositions and porosities, and are therefore expected to present different dielectric properties.

Transmission THz-TDS was used to determine their refractive index and absorption coefficient across the THz band. This technique relies on the generation and detection of single-cycle electromagnetic transients that cover the THz frequency band. The temporal waveform of such pulses is recorded and numerical algorithms are used to calculate their Fourier transform. The Fourier transform contains both the amplitude and phase information, which allows the calculation of the complex refractive index directly from the transmission measurements. The setup used is described in detail in [3] and the data processing in [8].

Interestingly, the real part of the refractive index for all the stones studied present negligible dispersion as shown in Fig. 1(a), and therefore the average values of the refractive index across this band are also included in Table 1. The absorption coefficient [shown in Fig. 1(b)] differs significantly between the various stones. The spectral dependence of the

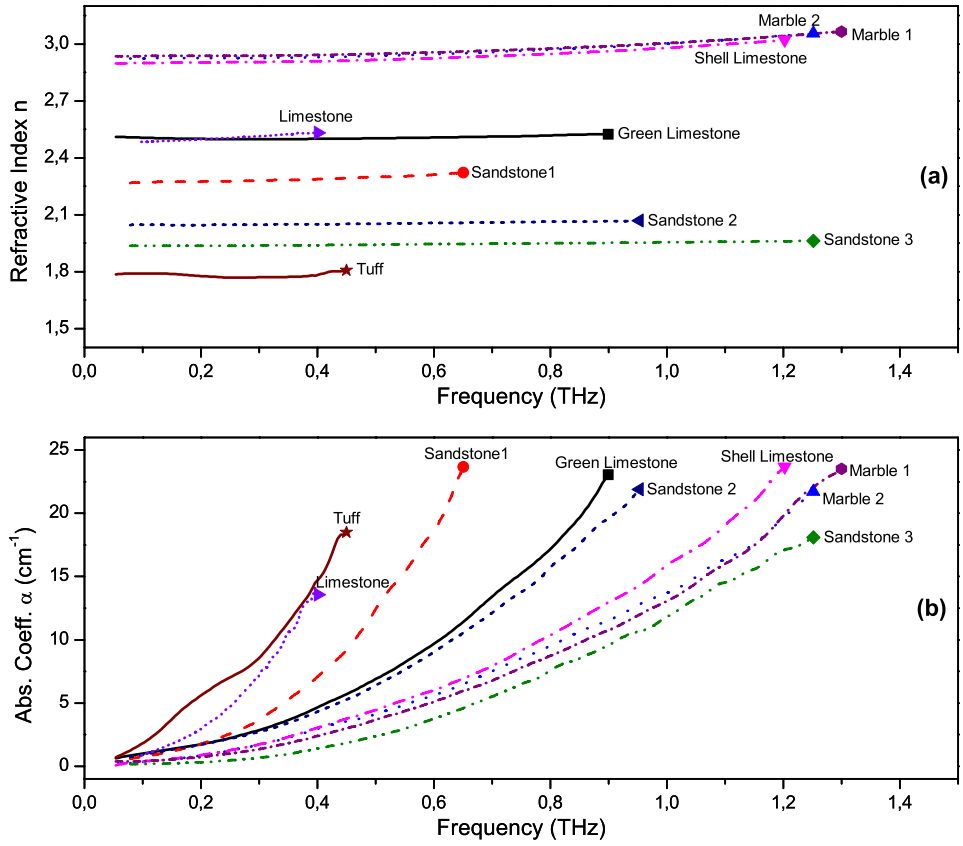


Fig. 1. (Color online) (a) Refractive index and (b) absorption coefficient of various stones used in artwork. The short names of the stones are indicated on the plot; the full names are listed in Table 1.

attenuation by all the samples presented is partly attributed to the absorption of the material itself and partly to scattering caused by the porosity of the different stones. All samples present an increasing absorption as function of frequency, which is typically expected for liquids and amorphous solids [9] and is consistent with previous measurements of similar samples [10]. The refractive indices and absorption coefficients are reported over different frequency intervals because the transmitted pulses had acceptable signal to noise ratio only in such spectral windows.

### 3. Reflection Spectroscopy

Terahertz time-of-flight measurements in a reflection geometry have been used before in order to locate and tomographically image objects of sizes larger than, or at least comparable to, the wavelengths of the pulses used [11]. We used the same technique to locate air gaps surrounded by stone. A setup similar to the one used is described in detail in [12]. In Figure 2, time-of-flight waveforms are presented for a single block of marble (type 2) of 3.7 mm thickness. The first distinguishable pulse (at $t = 20$ ps) is related to the Fresnel reflection at the entrance face of the stone. The second pulse is caused by the Fresnel reflection at the exit face of the stone sample. When a second piece of stone is located behind the first one, an additional pulse appears that corresponds to the Fresnel reflection at the entrance face of the second stone. In this fashion, subsequent interfaces in the radiation propagation direction can be assigned to reflection pulses further in the time-domain waveform. The temporal separation between pulses $\Delta t$ is proportional to the distance between interfaces

$$d = \frac{c\Delta t}{2n}, \tag{1}$$

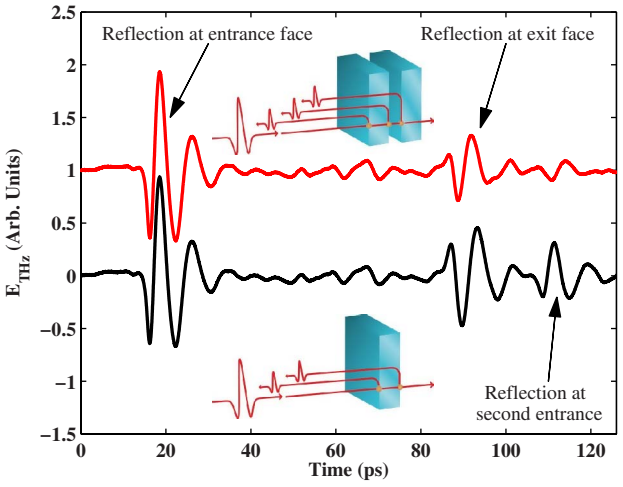


Fig. 2. (Color online) Two curves showing the reflected waveform of a single slab of stone as well as one slab followed by an air gap and a second piece of stone. The insets show illustrations to clarify the process.

where $c$ is the speed of light in vacuum and $n$ is the refractive index of the material between the two interfaces. Given that we have characterized the dielectric properties of the stone used in the measurements of Fig. 2, it is possible to determine the precise position of each interface if the pulses are well separated [13]. However, if either an air gap or a stone layer is too thin, the reflected pulses corresponding to the two interfaces overlap and the determination of their relative spacing becomes challenging.

In order to determine the smallest thickness that could be measured with a pulse of covering the 0 to 300 GHz band we performed a simple modeling of the THz reflection. We chose this spectral band as it is a region where the losses in most stones are relatively low and therefore it is possible to determine the existence of air gaps, cracks, or other features at reasonably large depths into the stone. A THz pulse that resembles the experimental ones we used can be modeled by

$$E(t) = A\frac{d^2}{dt^2}e^{-(t)^2/\tau^2}, \tag{2}$$

where $A$ is related to the amplitude of the pulse and $\tau$ is its temporal duration. Using this waveform the collection of reflections from a sample consisting of various layers of material can be modeled.

A refractive index of $n_s = 2.97$ that corresponds to marble 2, for which we have a reliable source of samples, was used to calculate the Fresnel transmission $(t_{as}, t_{sa})$ and reflection $(r_{as}, r_{sa})$ coefficients from air to stone and stone to air [14]. Using the Fresnel coefficients and the absorption coefficient for the stone which is $\alpha \sim 0.25$ cm$^{-2}$ at 200 GHz, the reflected waveform from an air–stone–air–stone layer system is expected to be

$$E_{\mathrm{THz}}(t) = r_{as}E\left(t - \frac{d_0}{c}\right) + \left[t_{as}r_{sa}t_{sa}E\left(t - \frac{d_0 + n_s d_1}{c}\right) + t_{as}^2 t_{sa}^2 r_{as}E\left(t - \frac{d_0 + n_s d_1 + d_2}{c}\right)\right]e^{-2\alpha d_1}, \tag{3}$$

where $d_0$ is an arbitrary distance between the THz setup and the face of the first sample, $d_1$ is the thickness of the first layer of stone, and $d_2$ is the thickness of the air gap between the two stones. In order to model a particular system. Eq. (3) was used for a first layer of stone of thickness $d_1 = 3.7$ mm, followed by air gaps of thicknesses 0, 0.1, 0.2, 0.4, 0.8, 1.6, and 3.2 mm. Given that at the moment we are concerned with the dependence of the THz reflection with the air gap thickness, the only part of the reflected waveform corresponding to the two interfaces around the gap is shown in Fig. 3(a). In the plot, it is possible to see that for air gap thicknesses of 1.6 mm and above, the two pulses corresponding to the exit interface of the first stone and the entrance interface of the second stone are clearly distinguishable. For shorter gaps, these two pulses overlap and it is not possible to separate them visually. Yet, if we examine the

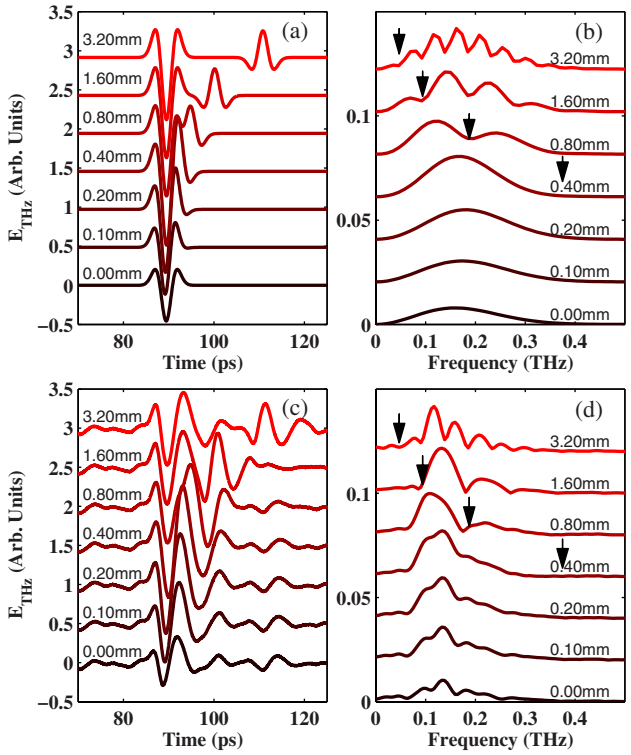


Fig. 3. (Color online) (a) Calculated THz time-domain pulses reflected at air gaps of different thicknesses. (b) Fourier transform of the data shown in (a); the arrows indicate the positions where the lowest frequency Fabry–Perot dips are expected for the air gap thickness modeled. (c) Experimental THz time-domain measurement of reflected pulses at an air gap between stones for various gap thicknesses. (d) Fourier transform of the data shown in (c); the arrows indicate the positions where the lowest frequency Fabry–Perot dips are expected for the nominal thickness of the air gaps.

Fourier transform corresponding to these waveforms [shown in Fig. 3(b)] it is possible to identify dips in the spectrum that correspond to Fabry–Perot oscillations. The frequency spacing between the Fabry–Perot spectral dips is

$$\nu_{\mathrm{FP}} = \frac{c}{2d_2}, \tag{4}$$

the lowest of these frequencies are indicated by arrows on the plot for each spectra. The spacing between such dips contains the information to determine the thickness of thinner gaps, for instance of 0.8 mm and down to about 0.5 mm. However smaller gaps cannot, in principle, be measured using the spectral Fabry–Perot dips unless the pulses are shorter, and therefore spectrally broader. A 3.7 mm stone sample followed by an air gap and a second (10 mm) stone sample system was prepared in the laboratory and reflection measurements were performed for the same air gap thicknesses modeled before. The time window that corresponds to the reflections of the two faces around the gap are shown in Fig. 3(c). The measured time-domain waveforms and spectra are consistent with the modeled ones. The corresponding spectra of this windowed waveforms is shown on Fig. 3(d), where it is possible to observe that the frequencies of the first Fabry–Perot dips correlate very well with the theoretical ones for each separation indicated by arrows.

Although it is not possible to find distinctive features in either the modeled or experimental time-domain waveforms or spectra for small gaps (<0.8 mm) that would allow us to quantify the thickness of the air gap, there is a dependence in the amplitude of the waveforms as function of gap thickness for both the modeled and experimental data sets. We decided to investigate if it is possible to obtain the thickness in this subwavelength regime by using the amplitude of these waveforms that result from the superposition of the reflections at the two interfaces around the air gap.

The first term of Eq. (3) does not depend on either the thickness of the first stone layer or on the thickness of the air gap, and therefore it can be used as a reference of the amplitude of the initial pulse. The second term, in square brackets, corresponds to the reflections at the second and third interfaces. This term does depend on the thickness of the air gap $d_2$. By integrating the absolute value of the time-domain waveform (shown in Fig. 4) over a window around the reflection of the first face $[a_1, a_2]$ and the reflections at the air gap $[b_1, b_2]$, we can obtain a parameter that measures the relative amplitude of these two reflections

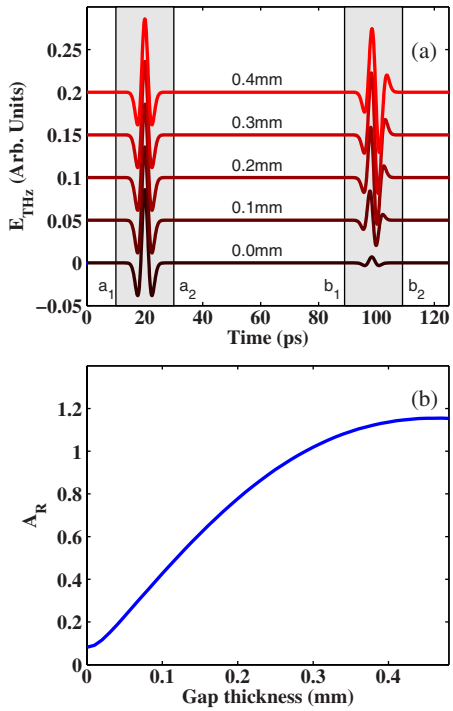


Fig. 4. (Color online) (a) Reflected time-domain waveforms for small air gaps. The amplitude of the reflection caused by the gap has a strong dependence with gap size in this regime. The integration windows $[a_1, a_2]$ and $[b_1, b_2]$ used to calculate the parameter $A_R$ are indicated. (b) The parameter $A_R$ as function of gap thickness.

$$A_R = \frac{\int_{a_1}^{a_2} |E_{\mathrm{THz}}(t)|\mathrm{d}t}{\int_{b_1}^{b_2} |E_{\mathrm{THz}}(t)|\mathrm{d}t}. \quad (5)$$

The calculation for this parameter is shown in Fig. 4(b). This plot indicates that $A_R$ is a bijective function, at least in this interval of thicknesses, and therefore it is possible to invert it in order to obtain the thickness from the parameter $A_R$.

In order to test if the thickness of a real air gap can be measured, a varying air gap was constructed by placing a 0.3 mm spacer between the two stone plates in one edge of the stones and no spacer on the opposite edge. This resulted in a wedged air gap between the stones with thicknesses varying from 0 to 0.3 mm depending on the position (see inset on the left of Fig. 5). The stones were placed on a two-axis stage in order to produce a collection of reflected THz waveforms for a mesh of points across the surface of the stones $(x,y)$. A three-dimensional reconstruction of the air gap thickness is presented in Fig. 5. An iterative algorithm adjusted the magnitude of $d_2$ in Eq. (3) in order to match the parameter $A_R$ calcuated from the experimental data. Only the points 6 mm away from the edges are shown in order to avoid artifacts caused by the clipping of the THz radiation at the borders of the sample. The surface in Fig. 5 shows that the thickness has an almost linear increase with position in the $x$ direction, while there is almost no variation in the $y$ direction as would be expected owing to the wedge shape of the gap.

The inset on the right hand side of Fig. 5 shows a cut at the central position in the $y$ direction. It is possible to observe that the thickness not only follows a qualitatively linear behavior but also that the size of the gap matches reasonably well the expected thickness for the different positions which are indicated by a dashed line. The deviations from the expected flat geometry can be attributed to two main sources. First, the stone is imperfectly cut so the surface is not entirely flat, second, the stone is not homogeneous

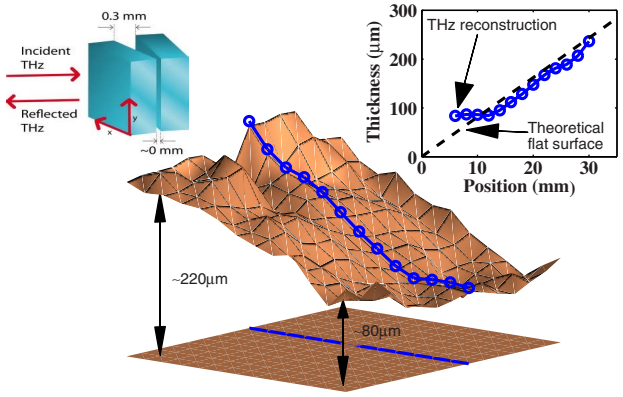


Fig. 5. (Color online) Three-dimensional reconstruction of a subwavelength wedged air gap between two pieces of stone. The inset on the left hand side illustrates the wedge gap geometry. The inset on the right hand side presents the thickness extracted from the THz measurement (circles) at the central position in the $y$ direction. The thickness of a perfect plane is indicated for comparison by a dashed line.

and therefore its refractive index changes slightly with position. For gaps thinner than 80 μm, the measurement deviates from the expected thickness. We attribute this mostly to the "ringing" in the time-domain signal caused by the presence of water vapor. We determined that the $A_R$ of a reflection-free water vapor signal corresponds to an air gap of approximately 70 μm. It would be possible to avoid this limitation by placing the spectroscopy system and sample in a dry atmosphere, such as nitrogen or vacuum; however, this would make it impractical for most real-world applications.

## 4. Conclusions

We presented the dielectric properties of various types of stones, which are of interest to artwork conservationists. We investigated the possibility of using time-of-flight reflection spectroscopy, in the 0 to 300 GHz band ($\lambda > 1$ mm), in order to locate and measure air gaps surrounded by a type of marble stone. Given that fractures in sculptures and historically relevant buildings made of stones are typically in the submillimeter thickness scale, we developed a method to three-dimensionally image such voids. We successfully tested this method for air gaps as small as ~80 μm (i.e., $<\lambda/10$). This technique can also be applied for the three-dimensional tomographic imaging of subwavelength fractures in many dielectric materials for quality control, artwork restoration, and structural damage evaluation on historical or modern buildings, among other purposes, in the future. This method could, in principle, be extended to the near infrared, visible, and ultraviolet by using ultrashort laser pulses.

The authors would like to thank the Deutsche Bundesstiftung Umwelt (Germany) for their financial support.

## References

1. G. Demortier and J. Ruvalcaba-Sil, "Quantitative ion beam analysis of complex gold-based artefacts," Nucl. Instr. Methods B **239**, 1–15 (2005).
2. P. Vandenabeele, F. Verpoort, and L. Moens, "Non-destructive analysis of paintings using fourier transform raman spectroscopy with fibre optics," J. Raman Spectrosc. **32**, 263–269 (2001).
3. P. U. Jepsen, D. G. Cooke, and M. Koch, "Terahertz spectroscopy and imaging - modern techniques and applications," Laser Photon. Rev. **5**, 124–166 (2011).
4. J. Jackson, J. Bowen, G. Walker, J. Labaune, G. Mourou, M. Menu, and K. Fukunaga, "A survey of terahertz applications in cultural heritage conservation science," IEEE Trans. THz Sci. Technol. **1**, 220–231 (2011).
5. K. Fukunaga, Y. Ogawa, S. Hayashi, and I. Hosako, "Terahertz spectroscopy for art conservation," IEICE Electron. Exp. **4**, 258–263 (2007).
6. A. Adam, P. Planken, S. Meloni, and J. Dik, "Terahertz imaging of hidden paint layers on canvas," Opt. Express **17**, 3407–3416 (2009).
7. K. Fukunaga, Y. Ogawa, S. Hayashi, and I. Hosako, "Application of terahertz spectroscopy for character recognition in a medieval manuscript," IEICE Electron. Exp. **5**, 223–228 (2008).
8. E. Castro-Camus and M. B. Johnston, "Extraction of the anisotropic dielectric properties of materials from polarization-resolved terahertz time-domain spectra," J. Opt. A **11**, 105206 (2009).

9. S. Taraskin, S. Simdyankin, S. Elliott, J. Neilson, and T. Lo, "Universal features of terahertz absorption in disordered materials," Phys. Rev. Lett. **97**, 55504 (2006).
10. R. Piesiewicz, C. Jansen, S. Wietzke, D. Mittleman, M. Koch, and T. Kürner, "Properties of building and plastic materials in the THz range," Int. J. Infrared Millim. Waves **28**, 363–371 (2007).
11. D. Mittleman, S. Hunsche, L. Boivin, and M. Nuss, "T-ray tomography," Opt. Lett. **22**, 904–906 (1997).
12. D. M. Mittleman, R. H. Jacobsen, and M. C. Nuss, "T-ray imaging," IEEE J. Sel. Top. Quantum Electron. **2**, 679–692 (1996).
13. O. Peters, S. Wietzke, C. Jansen, M. Scheller, and M. Koch, "Nondestructive detection of delaminations in plastic weld joints," in *35th International Conference on Infrared Millimeter and Terahertz Waves (IRMMW-THz)* (IEEE, 2010), pp. 1–2.
14. G. Fowles, *Introduction to Modern Optics* (Dover, 1989).